Letter | Editors' Suggestion

Search for beyond-mean-field signatures in heavy-ion fusion reactions

R. T. deSouza [1,*] K. Godbey [2,†] S. Hudan [1,‡] and W. Nazarewicz [3,§]

[1]*Department of Chemistry and Center for Exploration of Energy and Matter, Indiana University, Bloomington, Indiana 47408, USA*

[2]*FRIB Laboratory, Michigan State University, East Lansing, Michigan 48824, USA*

[3]*Department of Physics and Astronomy and FRIB Laboratory, Michigan State University, East Lansing, Michigan 48824, USA*

(Received 24 September 2023; revised 4 November 2023; accepted 14 February 2024; published 1 April 2024)

Examination of high-resolution, experimental fusion excitation functions for $^{16,17,18}\mathrm{O}+^{12}\mathrm{C}$ reveals a remarkable irregular behavior that is rooted in the structure of both the colliding nuclei and the quasimolecular composite system. The impact of the ℓ-dependent fusion barriers is assessed using a time-dependent Hartree-Fock model, viewed as a mean-field reference. Barrier penetrabilities, taken directly from a density-constrained calculation, provide a significantly improved description of the experimental data as compared to the standard Hill-Wheeler approach. The remaining deviations between the parameter-free theoretical mean-field predictions and experimental fusion cross sections are exposed and discussed.

DOI: 10.1103/PhysRevC.109.L041601

Introduction. The merging of two nuclei can provide a window into nuclear dynamics on short timescales. Heavy-ion fusion is governed by the interaction of the colliding nuclei resulting from the delicate time-dependent balance of the repulsive electrostatic force and the attractive nuclear force in the presence of angular momentum for non-central collisions. Of fundamental importance in describing heavy-ion fusion is the collective potential of the two colliding nuclei, collective excitations of projectile and target, and the appearance of clustering effects during the fusion process. Progress in experiment, theory, and high performance computing allows a direct confrontation of high-resolution fusion measurements with advanced time-dependent theoretical frameworks to provide new insights into fusion dynamics.

Experimental evidence. Indirect evidence for the transient configurations in fusion was first provided by examination of elastic scattering in $^{12}\mathrm{C}+^{12}\mathrm{C}$ [1]. Irregular energy dependence of the elastic cross section was interpreted as the formation of "molecular states" at specific energies. This behavior was attributed to the deformability of the carbon nuclei [2]. Absence of such behavior in $^{16}\mathrm{O}+^{16}\mathrm{O}$ [1] was interpreted in terms of the reduced deformability of the tightly bound, doubly magic $^{16}\mathrm{O}$ nucleus [2]. A direct examination of the fusion excitation function for $^{12}\mathrm{C}+^{12}\mathrm{C}$ [3], $^{16}\mathrm{O}+^{12}\mathrm{C}$ [4,5], $^{16}\mathrm{O}+^{16}\mathrm{O}$ [6,7], and $^{20}\mathrm{Ne}+^{20}\mathrm{Ne}$ [8] reveals the presence of an oscillatory structure in the near-barrier regime. Two factors contribute to the nonsmooth dependence of the fusion cross section on energy, namely the accumulation of cross section associated with successive individual ℓ waves with slightly different barriers [9–12] and the presence of resonances. In order to directly probe the contribution of transient configurations to the fusion cross section, particularly those that are weakly populated, it is crucial to provide an accurate description of the underlying mean-field component. An accurate description necessarily includes the contribution due for example, to ℓ-wave dependent barriers. The aim of the present work is to examine how an accurate description of the mean-field contribution to the fusion excitation function evolves with neutron number in comparison with experimental data. To accomplish this, we utilize high-resolution experimental data to confront state-of-the-art time-dependent Hartree-Fock (TDHF) calculations.

High-resolution fusion excitation functions were obtained both by using recent active-target measurements as well as by combining prior thin-target measurements. Fusion was identified either by the direct detection of the heavy fusion products following de-excitation or by their secondary γ emission. Any contribution from breakup prior to fusion, expected to be small for the energies and systems considered in this work, is not accounted for. Obtaining these high-resolution excitation functions was the key first step in this work.

Comparison of fusion processes induced by $^{16,17,18}\mathrm{O}$ nuclei provides insight into three highly interesting cases. The $^{16}\mathrm{O}$ represents the reference case of a doubly magic, tightly bound nucleus. In the case of $^{17}\mathrm{O}$, an odd unpaired neutron occupies the $0d_{5/2}$ shell, resulting in a ground-state spin $5/2^+$. The extent to which this valence neutron is strongly or weakly coupled to the core is expected to impact the fusion cross section. In the case of $^{18}\mathrm{O}$, the two valence neutrons form a Cooper pair. Pairing correlations are expected to impact the fusion cross section in two ways: by increasing the fusion barrier and by enhancing the neutron pair transfer. The experimental excitation functions for $^{16,17,18}\mathrm{O}+^{12}\mathrm{C}$ are presented in Fig. 1.

Direct comparison of these three experimental excitation functions alone provides considerable information. While the

*Corresponding author: desouza@iu.edu
†godbey@frib.msu.edu
‡shudan@indiana.edu
§witek@frib.msu.edu

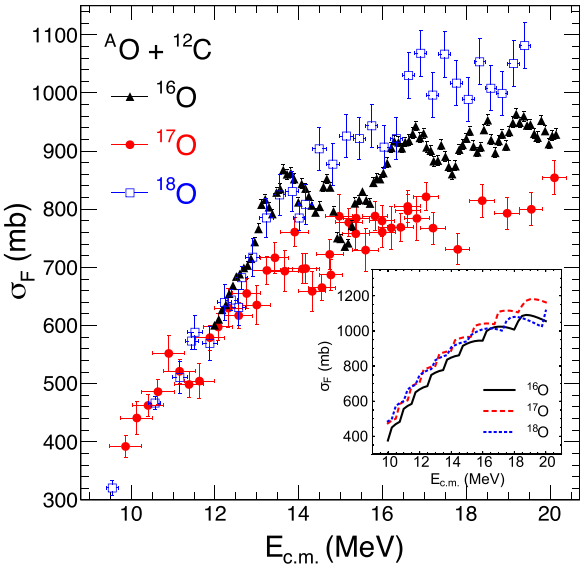

FIG. 1. Experimental fusion excitation functions for the reactions of ^{16}O (black triangles) [13], ^{17}O (red dots) [14], and ^{18}O (open squares) [15,16] impinged on a ^{12}C target. The inset shows the results of TDHF*. See text for details.

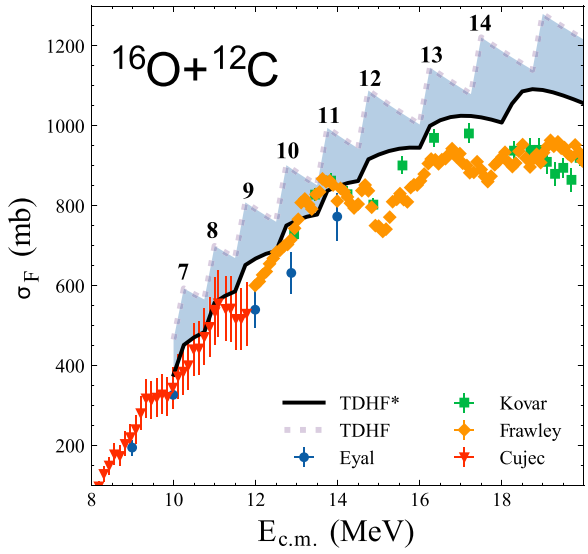

FIG. 2. Comparison of experiment with theory for the fusion excitation function for the $^{16}O + ^{12}C$ reaction. Experimental data are taken from Refs. [18] (blue circles), [5] (green squares), [13] (orange diamonds), and [19] (red upside-down triangles). Raw TDHF results are shown with a light dotted line and modified DC-TDHF/TDHF hybrid results are shown with a solid black line. The difference between TDHF and TDHF* is highlighted by shading. The values of $\ell(E_{c.m.})$ computed in TDHF are marked.

excitation functions exhibit common features, notable differences exist. All the excitation functions shown in Fig. 1 manifest a zigzag behavior superimposed on the overall increase in cross section with increasing energy. Significantly more structure is observed for ^{16}O with prominent peaks observed at $E_{c.m.} \approx 11$ MeV, 14 MeV, and 16.5 MeV. The magnitude of these peaks is reduced for ^{17}O and ^{18}O. At lower energies, all the excitation functions are rather similar.

In contrast, the reduction in cross section for ^{17}O as compared to ^{16}O at higher energies is particularly noteworthy. If the valence neutron in ^{17}O is weakly coupled to the ^{16}O core one might expect either an increased fusion cross section due to an increased spatial extent of the neutrons or essentially no increase at all if neutron breakup preceded fusion. The reduction of the fusion cross section for ^{17}O thus suggests that in this energy regime the presence of the valence neutron does influence fusion. This influence could be associated with the increased role of breakup and neutron transfer which can suppress the above-barrier cross-section while enhancing the below-barrier cross section [17]. The enhanced fusion cross section at $E_{c.m.} > 14$ MeV for ^{18}O as compared to ^{16}O suggests that the effects due to pairing correlations are washed out at higher energies and the effect of the increased neutron radius dominates.

In order to provide the most complete, high-resolution description of the fusion excitation function for $^{16}O + ^{12}C$ several data sets have been combined and the result is presented in Fig. 2. The cross section at higher energies which relies on the direct detection of the fusion products [5,13,18] is augmented by indirect measurements of the cross section at lower incident energies [19]. Measurement of fusion at higher incident energies that relied on γ-ray measurements were excluded due to larger uncertainties. The reported cross sections depicted in Fig. 2 are internally very consistent. The high resolution data not only reveals the peaks in the cross section at $E_{c.m.} \approx 11$ MeV, 14 MeV, and 16.5 MeV previously noted but also an oscillatory behavior at lower energies.

Theoretical framework. As briefly mentioned before, there exist many theoretical approaches to studying fusion cross sections above and below the barrier. Coupled channels approaches, for instance, have been quite successful in describing the light-ion reactions of interest in this work [9,20]. In this study we have adopted the TDHF framework to understand the mean-field contribution to the fusion excitation functions for the above-barrier collisions. On general grounds, TDHF is a many-body approach that is well suited to describe the large-amplitude collective motion associated with fusion while also describing the transfer dynamics, equilibration processes, and Pauli blocking that affect heavy-ion fusion probabilities [21–23]. These effects are included self-consistently and no fits are performed beyond the original calibration of the energy density functional (EDF), representing the internucleon interaction, to static properties of nuclei. We emphasize that the interion (optical) potential that is the main source of uncertainty in coupled channel methods is obtained microscopically in TDHF from the EDF.

Recently, advances in theoretical and computational techniques have allowed TDHF calculations to be performed on a three-dimensional (3D) Cartesian grid thus eliminating artificial symmetry restrictions [24–27]. The unrestricted 3D geometry allows for precise simulations that can capture the rich time-dependent dynamics at play in light nuclear reactions [11,28]. Although in the sub-barrier regime it is necessary to perform density constrained TDHF (DC-TDHF) calculations [29,30] to obtain the heavy-ion potentials [11,31],

at the above-barrier energies considered in this work direct TDHF calculations can be performed by initiating collisions for a series of increasing impact parameters until the maximum impact parameter for fusion is reached. Moreover, the barrier associated with each incoming ℓ wave can be determined by finding the lowest energy associated with each ℓ window. This collision energy was scanned in steps of 0.25 MeV across the reported range of energies for all systems. The EDF employed in this work was primarily UNEDF1 [32], though a set of parameters chosen from the Bayesian posterior distribution [33] was also used to assess the sensitivity of the reaction outcomes to the choice of EDF [34]. With this EDF (and many others), the ^{12}C ground state is predicted to be spherical–a fact at odds with deformations deduced from alpha scattering measurements [35], or an expected contribution from three-α clustering configuration [36]. Some EDFs can reproduce an oblate-deformed ^{12}C [37,38] and constrained HF calculations can be used to prepare a clustering configuration [39], though the study in Ref. [40] of the $^{12}\mathrm{C}+{}^{12}\mathrm{C}$ reaction suggests the impact of deformation effects at energies considered in our study should be minor. This paired with the fact that we are considering ^{12}C as a common target in each reaction should result in a systematic deficiency across all systems and energies.

For the ^{18}O reaction the frozen pairing approximation was employed, as in Ref. [16]. In contrast to the variations seen in fusion studies for heavier nuclei [34,41], the above-barrier fusion cross sections have been found to be largely insensitive to the choice of effective interaction. While the unrestricted 3D Cartesian geometry affords a more flexible computational framework, it comes at an increased cost with each simulation requiring a few hours on a standard multicore compute node. For the entire study, considering three systems, around 3000 individual trajectories were simulated to precisely determine the capture cross sections across a wide range of impact parameters and energies above the barrier. Illustrative videos of the time evolution of the neutron localization function [42] obtained in our TDHF simulations can be found in the Supplemental Material [43].

The fusion cross section can be expressed as

$$\sigma = \frac{\pi\hbar^2}{2\mu E_{\mathrm{c.m.}}}\sum_{\ell=0}^{\ell_{\max}}(2\ell+1)P_\ell, \tag{1}$$

where μ is the reduced mass, $E_{\mathrm{c.m.}}$ is the center-of-mass energy, P_ℓ is the probability of the ℓ-wave fusing, and $\ell_{\max}$ corresponds to the largest ℓ wave that fuses. For the raw TDHF results, P_ℓ is 1 if the system fuses and 0 if it does not.

The TDHF calculations were performed for $6 < \ell \leqslant 20$. For each ℓ, a sharp increase in cross section is observed when the barrier for that particular ℓ wave is surpassed. Tunnelling through the barrier mitigates this sharp threshold behavior [11,12]. While the Hill-Wheeler approximation is often used for the penetrability, this approach presumes the transmission through an inverted parabolic potential. This assumption becomes progressively worse with increasing ℓ wave, particularly as ℓ approaches $\ell_{\max}$. In the current work, we extract P_ℓ directly from the penetrability of the computed DC-TDHF potentials for that ℓ value thus providing a consistent microscopic approach. In the event that $\ell_{\max}$ is different between the TDHF and DC-TDHF approaches, the lower of the two is chosen. In the following, we refer to this method as the hybrid DC-TDHF/TDHF approach and designate it TDHF*. The primary difference between TDHF* and the standard treatment for TDHF as detailed in Refs. [11,12] is that the cross sections are substantially suppressed for TDHF*.

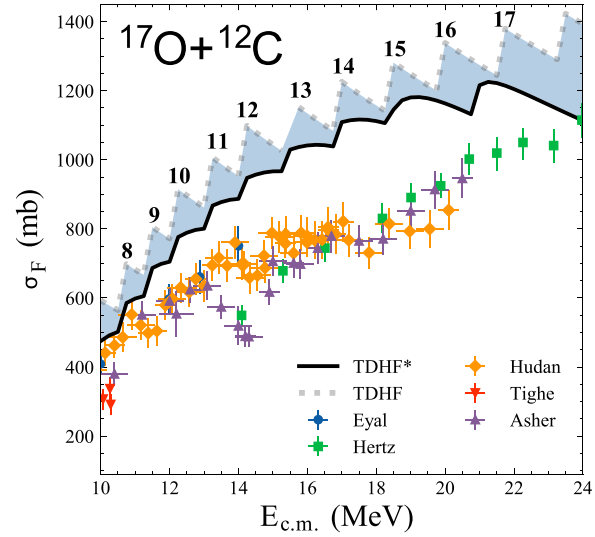

FIG. 3. Similar as in Fig. 2 but for the $^{17}\mathrm{O}+{}^{12}\mathrm{C}$ reaction. Experimental data are taken from Refs. [18] (blue circles), [45] (green squares), [14] (orange diamonds), [44] (red upside-down triangles), and [20] (purple triangles).

Discussion. The predictions of the TDHF* model for the three reactions considered are shown in the inset of Fig. 1. As might be naively expected from geometrical considerations based on mass scaling, ^{16}O exhibits a smaller cross section than ^{17,18}O. The predicted trend with neutron number differs from that of the experimental data shown in Fig. 1. The trend of the fusion cross section observed for the three systems is not reproduced by theory. At the highest bombarding energies, the $^{18}\mathrm{O}+{}^{12}\mathrm{C}$ system experimentally exhibits the largest fusion cross section, followed by $^{16}\mathrm{O}+{}^{12}\mathrm{C}$ and finally $^{17}\mathrm{O}+{}^{12}\mathrm{C}$. In contrast, theoretically, $^{17}\mathrm{O}+{}^{12}\mathrm{C}$ displays the largest cross section, while the cross sections for the $^{18}\mathrm{O}+{}^{12}\mathrm{C}$ and $^{16}\mathrm{O}+{}^{12}\mathrm{C}$ reactions are predicted to be similar.

More insight is provided by a direct and detailed comparison of the measured and calculated fusion excitation functions shown in Figs. 2–4. We first discuss the $^{16}\mathrm{O}+{}^{12}\mathrm{C}$ reaction as it provides an excellent reference due to the rigid nature of the ^{16}O projectile. As shown in Fig. 2, for $E_{\mathrm{c.m.}} < 14$ MeV, the TDHF* method provides a good description of the fusion excitation function due to the addition of successive ℓ waves. For $E_{\mathrm{c.m.}} > 11$ MeV, TDHF* systematically overestimates the measured excitation function, although the oscillating behavior of the cross section for $E_{\mathrm{c.m.}} < 11.5$ MeV is well reproduced. The raw TDHF method systematically overshoots the data.

Overestimation of the fusion cross section at higher energies by TDHF has typically been attributed to the existence

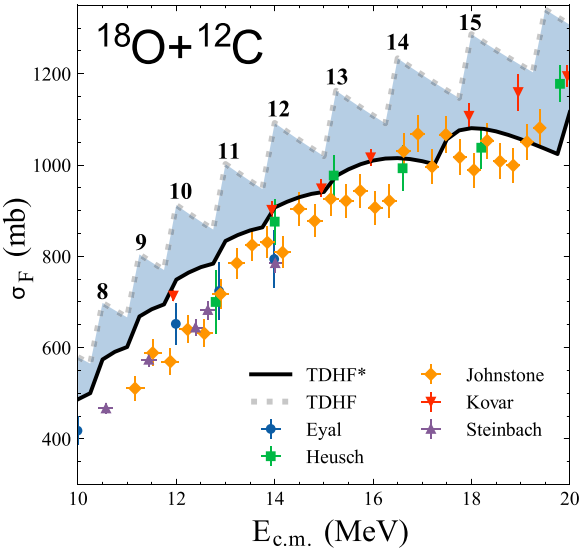

FIG. 4. Similar as in Fig. 2 but for the $^{18}O+^{12}C$ reaction. Experimental data are taken from Refs. [18] (blue circles), [49] (green squares), [15] (orange diamonds), [5] (red upside-down triangles), and [16] (purple triangles).

of breakup channels in the experimental data that are not properly represented in TDHF, though the full extent of this effect is an open question. Our TDHF* calculations indicate that a more accurate description of transmission probabilities reduces the need for invoking breakup channels. All in all, despite the overestimation of the cross section for $E_{c.m.} > 14$ MeV, we consider the description of the reference reaction $^{16}O+^{12}C$ by the parameter-free TDHF* approach to be quite satisfactory.

Having established the success of TDHF* in describing the $^{16}O+^{12}C$ reaction, we investigate the impact on fusion introduced by the addition of a single neutron to the projectile. Figure 3 illustrates the case of $^{17}O+^{12}C$. The experimental data were collected in recent active thick-target measurements [14,20] along with earlier thin-target measurements [18,44,45]. It is to be noted that the close examination of different experimental data sets for ^{17}O reveals some significant differences. For $E_{c.m.} \approx 14$ MeV the data of [20] and the lowest energy point from [45] suggest a pronounced dip in the cross section differing from the data of [14,18]. The accuracy of the thick-target data in Ref. [14] has been corroborated by comparing the measured cross-section with thin-target measurement of the fusion cross section of mirror nuclei. The magnitude of the dip at $E_{c.m.} \approx 14$ MeV is significantly reduced as compared to [20] and is shifted to slightly higher energy. Also, at the lowest energies shown, the data of Ref. [44] appear slightly low relative to the data from both [14,18] which are in a reasonable agreement. As the data of Ref. [14] are self-normalizing, in our opinion, they provide a more accurate measure of the fusion cross section.

The deviation from smooth behavior of the excitation function evident for the case of $^{16}O+^{12}C$, is also apparent in the case of the ^{17}O but the pronounced zigzag pattern in the cross section, as seen in the ^{16}O data, is harder to quantify. The TDHF* calculations for this reaction significantly overestimate the measured cross section for $14 < E_{c.m.} < 21$ MeV. There are several possible reasons for this, including neutron transfer which does not lead to fusion. The impact of transfer on the fusion probabilities was estimated by checking the isovector fusion potentials extracted from DC-TDHF in a similar procedure to Ref. [21]. As seen in Fig. S1 of [43], the magnitude of the isovector contribution for ^{17}O is less than that of ^{18}O, suggesting that any transfer effects at the mean-field level will not account for the significant suppression in above barrier cross sections seen in experiment. The presence of nucleonic cluster-like structures in the transient configurations can be probed by TDHF, see, e.g., [42]. However, the TDHF results shown in Fig. 1 do not show any appreciable reduction of σ_F for ^{17}O. On the contrary, the predicted cross section for ^{17}O systematically exceeds the ^{16}O "reference".

Since the odd neutron in ^{17}O occupies the $0d_{5/2}$ orbit leading to the $5/2^+$ ground state of ^{17}O, some increase of the fusion barrier may be possible due to a hindrance factor of fusion by specialization energy—an increase in the barrier due to angular momentum conservation [46]. This effect, considered for fission, has so far not been considered by theoretical approaches to heavy-ion fusion. In particular, it is not accounted for by TDHF which does not conserve the *total angular momentum* of the system, including the intrinsic angular momenta of colliding nuclei. An experimental argument against this scenario, however, is the similarity of the measured fusion excitation functions for ^{16}O and ^{17}O projectiles at low energies seen in Fig. 1. Let us also mention that the reduction of the fusion cross section for ^{17}O can be due to the coupling to the reaction channel involving the $1/2^+$ excited state of ^{17}O [47,48].

We now examine the impact of two valence neutrons in ^{18}O. The excitation function for $^{18}O+^{12}C$ shown in Fig. 4 utilizes thin-target measurements [16,18,49] together with recent active thick-target data [15]. While the experimental data exhibit oscillations, the presence of sharp resonant-like structures is absent. The TDHF* model with pairing provides a reasonably good overall agreement with the data although the calculations slightly overestimate the data.

Pairing correlations are expected to effectively increase the fusion barrier and thus decrease fusion cross sections [16,50,51]. The two additional neutrons, however are also expected to increase the radius of the nucleus (the difference between the root-mean-square matter radii of ^{18}O and ^{16}O calculated with UNEDF1 is about 0.1 fm, which is a 4% effect). and aid in neck formation—two effects that should serve to enhance to fusion cross sections. The experimental data in Fig. 1 show a similar behavior of cross sections for ^{16}O and ^{18}O at low energies, suggesting that any pairing effects are balanced by the other two mechanisms. At energies above 14 MeV, however, the fusion excitation function exceeds that of ^{16}O, indicating that the impact of pairing is less important than the projectile geometry, a feature expected as pairing correlations tend to erode at higher excitation energies. This also explains the better predictive performance for TDHF*

for the ^{18}O system at higher energies, as the model employs frozen pairing.

Summary. We have presented a framework for using a microscopic, parameter-free TDHF* model to investigate fusion excitation functions in the oxygen isotopes. To obtain $\sigma_F(E)$ with sufficient resolution, multiple experimental data sets were combined. The resulting data reveal oscillatory structures consistent with the presence of different ℓ-wave barriers. To accurately describe the experimental data, an extension of the standard TDHF approach was required to calculate the fusion penetrability directly from the DC-TDHF potential. The resulting TDHF* model provided a reasonably good description for the reference case of the ^{16}O-induced fusion, including the reproduction of oscillatory structures. A slightly worse, but still acceptable agreement with experiment was obtained for ^{18}O-induced fusion. An appreciable reduction of the experimental fusion excitation function for ^{17}O remains a puzzle.

Several possible explanations exist for the remaining discrepancies between experiment and theory: the effect of breakup and transfer channels, an imperfect description of ℓ-dependent fusion barriers by TDHF, or the presence of transient configurations involving nucleonic clusters. Distinguishing between these possibilities requires advances on both experimental and theoretical fronts. Systematic high-resolution, exclusive measurements of heavy-ion fusion and transfer/breakup measurements along isotopic chains is necessary in order to establish the limits of breakup and transfer channels. This experimental data, paired with continued investment in high-performance computing, will be critical in enabling the development of a more complete beyond-mean-field description of heavy-ion fusion.

Acknowledgments. This work was supported by the U.S. Department of Energy Office of Science under Grants No. DE-FG02-88ER-40404 (Indiana University), DOE-DE-SC0013365 and DE-SC0023175 (Michigan State University), and DOE-DE-NA0004074 (NNSA, the Stewardship Science Academic Alliances program). This work was supported in part through computational resources and services provided by the Institute for Cyber-Enabled Research at Michigan State University.

[1] D. Bromley, J. Kuehner, and E. Almquist, Resonant elastic scattering of ^{12}C by carbon, Phys. Rev. Lett. **4**, 365 (1960).
[2] E. Vogt and H. McManus, "Molecular" states formed by two carbon nuclei, Phys. Rev. Lett. **4**, 518 (1960).
[3] P. Sperr, T. H. Braid, Y. Y. Eisen, D. G. Kovar, F. W. Prosser, J. P. Schiffer, S. L. Tabor, and S. Vigdor, Fusion cross sections of light heavy-ion systems: Resonances and shell effects, Phys. Rev. Lett. **37**, 321 (1976).
[4] P. Sperr, S. Vigdor, Y. Eisen, W. Henning, D. G. Kovar, T. Ophel, and B. Zeidman, Oscillations in the excitation function for complete fusion of ^{16}O + ^{12}C, Phys. Rev. Lett. **36**, 405 (1976).
[5] D. G. Kovar *et al.*, Systematics of carbon- and oxygen-induced fusion on nuclei with $12 \leqslant A \leqslant 19$, Phys. Rev. C **20**, 1305 (1979).
[6] B. Fernandez, C. Gaarde, J. Larsen, S. Pontoppidan, and F. Videbaek, Fusion cross sections for the ^{16}O + ^{16}O reaction, Nucl. Phys. A **306**, 259 (1978).
[7] J. J. Kolata, R. M. Freeman, F. Haas, B. Heusch, and A. Gallmann, Gross and intermediate-width structure in the interaction of ^{16}O with ^{16}O, Phys. Rev. C **19**, 2237 (1979).
[8] I. Tserruya, Y. Eisen, D. Pelte, A. Gavron, H. OeschIer, D. Berndt, and H. L. Harney, Total fusion cross section for the ^{16}O + ^{16}O system, Phys. Rev. C **18**, 1688 (1978).
[9] H. Esbensen, Structures in high-energy fusion data, Phys. Rev. C **85**, 064611 (2012).
[10] C. Y. Wong, Reaction cross sections in heavy-ion collisions, Phys. Rev. C **86**, 064603 (2012).
[11] C. Simenel, R. Keser, A. S. Umar, and V. E. Oberacker, Microscopic study of ^{16}O + ^{16}O fusion, Phys. Rev. C **88**, 024617 (2013).
[12] N. Rowley and K. Hagino, Examination of fusion cross sections and fusion oscillations with a generalized Wong formula, Phys. Rev. C **91**, 044617 (2015).
[13] A. D. Frawley, N. R. Fletcher, and L. C. Dennis, Resonances in the ^{16}O + ^{12}C fusion cross section between $E_{c.m.} = 12$ and 20 MeV, Phys. Rev. C **25**, 860 (1982).
[14] S. Hudan, J. E. Johnstone, R. Kumar, R. T. deSouza, J. Allen, D. W. Bardayan, D. Blankstein, C. Boomershine, S. Carmichael, A. Clark, S. Coil, S. L. Henderson, P. D. O'Malley, and W. W. von Seeger, Quantifying resonance behavior in the fusion of ^{17}O with ^{12}C at above-barrier energies, Phys. Rev. C **107**, 064612 (2023).
[15] J. Johnstone *et al.*, Improving the characterization of fusion in a MuSIC detector by spatial localization, Nucl. Instrum. Methods Phys. Res. A **1025**, 166212 (2021).
[16] T. K. Steinbach, J. Vadas, J. Schmidt, C. Haycraft, S. Hudan, R. T. deSouza, L. T. Baby, S. A. Kuvin, I. Wiedenhöver, A. S. Umar, and V. E. Oberacker, Sub-barrier enhancement of fusion as compared to a microscopic method in ^{18}O + ^{12}C, Phys. Rev. C **90**, 041603(R) (2014).
[17] F. Gollan, D. Abriola, A. Arazi, M. A. Cardona, E. de Barbar´, J. de Jesús, D. Hojman, R. M. Id Betan, J. Lubian, A. J. Pacheco, B. Paes, D. Schneider, and H. O. Soler, One-neutron transfer, complete fusion, and incomplete fusion from the ^{9}Be + ^{197}Au reaction, Phys. Rev. C **104**, 024609 (2021).
[18] Y. Eyal, M. Beckerman, R. Chechik, Z. Fraenkel, and H. Stocker, Nuclear size and boundary effects on fusion barrier of oxygen with carbon, Phys. Rev. C **13**, 1527 (1976).
[19] B. Čujec and C. Barnes, Total reaction cross section for ^{12}C + ^{16}O below the Coulomb barrier, Nucl. Phys. A **266**, 461 (1976).
[20] B. Asher, S. Almaraz-Calderon, K. Kemper, L. Baby, E. Lopez-Saavedra, A. Morelock, J. Perello, V. Tripathi, and N. Keeley, Resolution of a long-standing discrepancy in the ^{17}O + ^{12}C fusion excitation function, Eur. Phys. J. A **57**, 272 (2021).
[21] K. Godbey, A. S. Umar, and C. Simenel, Dependence of fusion on isospin dynamics, Phys. Rev. C **95**, 011601(R) (2017).
[22] C. Simenel, K. Godbey, and A. S. Umar, Timescales of quantum equilibration, dissipation and fluctuation in nuclear collisions, Phys. Rev. Lett. **124**, 212504 (2020).
[23] C. Simenel, A. S. Umar, K. Godbey, M. Dasgupta, and D. J. Hinde, How the pauli exclusion principle affects

fusion of atomic nuclei, Phys. Rev. C **95**, 031601(R) (2017).
[24] A. S. Umar, M. R. Strayer, J.-S. Wu, D. J. Dean, and M. C. Güçlü, Nuclear Hartree-Fock calculations with splines, Phys. Rev. C **44**, 2512 (1991).
[25] K.-H. Kim, T. Otsuka, and P. Bonche, Three-dimensional TDHF calculations for reactions of unstable nuclei, J. Phys. G **23**, 1267 (1997).
[26] A. S. Umar and V. E. Oberacker, Time-dependent response calculations of nuclear resonances, Phys. Rev. C **71**, 034314 (2005).
[27] J. A. Maruhn, P. G. Reinhard, P. D. Stevenson, J. R. Stone, and M. R. Strayer, Dipole giant resonances in deformed heavy nuclei, Phys. Rev. C **71**, 064328 (2005).
[28] K. Godbey, C. Simenel, and A. S. Umar, Absence of hindrance in microscopic $^{12}\mathrm{C} + {}^{12}\mathrm{C}$ fusion study, Phys. Rev. C **100**, 024619 (2019).
[29] A. S. Umar, V. E. Oberacker, and C. J. Horowitz, Microscopic sub-barrier fusion calculations for the neutron star crust, Phys. Rev. C **85**, 055801 (2012).
[30] R. T. deSouza, S. Hudan, V. E. Oberacker, and A. S. Umar, Confronting measured near- and sub-barrier fusion cross sections for $^{20}\mathrm{O} + {}^{12}\mathrm{C}$ with a microscopic method, Phys. Rev. C **88**, 014602 (2013).
[31] A. S. Umar and V. E. Oberacker, Heavy-ion interaction potential deduced from density-constrained time-dependent Hartree-Fock calculation, Phys. Rev. C **74**, 021601(R) (2006).
[32] M. Kortelainen, J. McDonnell, W. Nazarewicz, P.-G. Reinhard, J. Sarich, N. Schunck, M. V. Stoitsov, and S. M. Wild, Nuclear energy density optimization: Large deformations, Phys. Rev. C **85**, 024304 (2012).
[33] J. D. McDonnell, N. Schunck, D. Higdon, J. Sarich, S. M. Wild, and W. Nazarewicz, Uncertainty quantification for nuclear density functional theory and information content of new measurements, Phys. Rev. Lett. **114**, 122501 (2015).
[34] K. Godbey, A. S. Umar, and C. Simenel, Theoretical uncertainty quantification for heavy-ion fusion, Phys. Rev. C **106**, L051602 (2022).
[35] M. Yasue, T. Tanabe, F. Soga, J. Kokame, F. Shimokoshi, J. Kasagi, Y. Toba, Y. Kadota, T. Ohsawa, and K. Furuno, Deformation parameter of $^{12}\mathrm{C}$ via $^{12}\mathrm{C}(\alpha, \alpha')$ and $^{12}\mathrm{C}(\alpha, \alpha'\alpha)$ reactions, Nucl. Phys. A **394**, 29 (1983).
[36] M. Freer, H. Horiuchi, Y. Kanada-En'yo, D. Lee, and Ulf-G. Meißner, Microscopic clustering in light nuclei, Rev. Mod. Phys. **90**, 035004 (2018).
[37] J. P. Svenne and R. S. Mackintosh, Spin-orbit force and the deformation of $^{12}\mathrm{C}$, Phys. Rev. C **18**, 983 (1978).
[38] W. Long, J. Meng, N. Van Giai, and S.-G. Zhou, New effective interactions in relativistic mean field theory with nonlinear terms and density-dependent meson-nucleon coupling, Phys. Rev. C **69**, 034319 (2004).
[39] A. S. Umar, K. Godbey, and C. Simenel, Cluster model of $^{12}\mathrm{C}$ in the density functional theory framework, Phys. Rev. C **107**, 064605 (2023).
[40] V. Y. Denisov and N. A. Pilipenko, Fusion of deformed nuclei: $^{12}\mathrm{C} + {}^{12}\mathrm{C}$, Phys. Rev. C **81**, 025805 (2010).
[41] P.-G. Reinhard, A. S. Umar, P. D. Stevenson, J. Piekarewicz, V. E. Oberacker, and J. A. Maruhn, Sensitivity of the fusion cross section to the density dependence of the symmetry energy, Phys. Rev. C **93**, 044618 (2016).
[42] B. Schuetrumpf and W. Nazarewicz, Cluster formation in precompound nuclei in the time-dependent framework, Phys. Rev. C **96**, 064608 (2017).
[43] See Supplemental Material at http://link.aps.org/supplemental/10.1103/PhysRevC.109.L041601 for videos of the time evolution of the neutron localization function for the collision of $^{16,17}\mathrm{O} + {}^{12}\mathrm{C}$ and a figure of the isovector part of the DC-TDHF potential for the $^{16,17,18}\mathrm{O} + {}^{12}\mathrm{C}$ reaction.
[44] R. J. Tighe, J. J. Kolata, M. Belbot, and E. F. Aguilera, Possible signatures of nuclear-molecular formation in O+C systems, Phys. Rev. C **47**, 2699 (1993).
[45] A. Hertz, H. Essel, H. J. Körner, K. E. Rehm, and P. Sperr, Maximum fusion cross section for the system $^{12}\mathrm{C} + {}^{17}\mathrm{O}$, Phys. Rev. C **18**, 2780(R) (1978).
[46] S. Hofmann, F. P. Heßberger, V. Ninov, P. Armbruster, G. Münzenberg, C. Stodel, A. G. Popeko, A. V. Yeremin, S. Saro, and M. Leino, Excitation function for the production of $^{265}108$ and $^{266}109$, Z. Phys. A **358**, 377 (1997).
[47] R. M. Freeman, C. Beck, F. Haas, A. Morsad, and N. Cindro, $^{12}\mathrm{C} + {}^{17}\mathrm{O}$ reaction, Phys. Rev. C **33**, 1275 (1986).
[48] C. Beck, R. Freeman, F. Haas, B. Heusch, and J. Kolata, Role of the valence neutron in the $^{12}\mathrm{C} + {}^{17}\mathrm{O}$ and $^{13}\mathrm{C} + {}^{16}\mathrm{O}$ collisions, Nucl. Phys. A **443**, 157 (1985).
[49] B. Heusch, C. Beck, J. P. Coffin, P. Engelstein, R. M. Freeman, G. Guillaume, F. Haas, and P. Wagner, Entrance channel effect for complete fusion of O + C isotopes, Phys. Rev. C **26**, 542 (1982).
[50] P. Magierski, K. Sekizawa, and G. Wlazłowski, Novel role of superfluidity in low-energy nuclear reactions, Phys. Rev. Lett. **119**, 042501 (2017).
[51] P. Magierski, A. Makowski, M. C. Barton, K. Sekizawa, and G. Wlazłowski, Pairing dynamics and solitonic excitations in collisions of medium-mass, identical nuclei, Phys. Rev. C **105**, 064602 (2022).